Fire design verification of an immersed tunnel using nonlinear analysis

Rafael Sanabria Díaz [1] , Eva Lantsoght [1, 2] , Max A.N. Hendriks [1, 3]

[1] Faculty of Civil Engineering and Geosciences, Delft University of Technology Delft, the Netherlands

[2] College of Sciences and Engineering, Universidad San Francisco de Quito, Quito, Ecuador

[3] Department of Structural Engineering, Norwegian University of Science and Technology, Trondheim, Norway

Fire design is an accidental loading case requiring verification against the ultimate limit state (ULS). Different to other types of loads, fire cannot be represented as a static load; rather, it consists of indirect effects caused by differential or restrained thermal expansion, which typically can only be estimated through advanced methods. This study proposes a procedure to verify the fire resistance and residual capacity of concrete structures using nonlinear finite element analysis (NLFEA). A staggered approach is employed within this procedure to couple transient thermal and mechanical analyses. The method is applied to estimate the fire resistance and residual capacity of a reinforced concrete (RC) as a function of the time exposure. For demonstration purposes a case study has been defined which is inspired by typical rectangular cross-section widely use in the Netherlands for immersed tunnels. Results indicate that the numerical models effectively trace damage and stress development during the fire event, confirming a significant thermal gradient across the thickness of the concrete section. The study concludes that these indirect effects must be addressed in the fire design of tunnels, even if fire protection is used.

Keywords: Fire, immersed tunnels, nonlinear analysis, finite element method, reinforced concrete

1 Introduction

Immersed tunnels play a crucial role in the transportation infrastructure in the Netherlands. The adoption of this tunnel technique was motivated by a growing traffic congestion problem across the road network during the 1930s. To meet this demand, the

Netherlands needed to build many relatively short waterway crossings. Building additional bridges was only partially feasible, as it would require the construction of long approach structures in the flat landscape and low-lying delta regions in the country. All these circumstances led to the construction of the Maastunnel in Rotterdam, the first Dutch immersed tunnel, opened in 1942. Since then, several more tunnels using this method have been built across the Netherlands.

Similarly to other types of tunnels, immersed tunnels are prone to undesired events such as fire or explosions. In the Netherlands, the need for enhanced fire safety measures became evident in 1978 after a fire in the Velsertunnel. This incident promoted further studies commissioned by Rijkswaterstaat (Dutch Ministry of Transport and Water Management, RWS). The research aimed to determine the maximum thermal load on the tunnel structure due to the worst possible fire scenario in a tunnel. The fire scenario was based on the following assumptions: a crash with a 50 m^3 petrol tanker, a pool size of 150 m^2 , a maximum heat release of 300 MW, and a leakage for about 90-120 minutes. Based on the research findings, the RWS fire curve was developed, and passive fire protection measures, such as heat-resistant cladding, were implemented in immersed tunnels.

Despite the advances in fire engineering in the last decades, the structural behaviour of reinforced concrete (RC) tunnels subjected to high temperatures is not fully understood. This is evident in many current design standards, which rely on simplified verification methods that cannot predict the structural capacity of RC tunnels during and after fire events. As a result, quantifying the safety margin of an RC structure against a specific fire scenario remains challenging. To address this, alternative design approaches, such as performance-based design (PBD), have gained popularity in recent years for verifying the fire resistance of structures. PBD allows for more realistic scenario modelling and provides innovative solutions aligned with specific performance objectives (Van Coile et al., 2022; Gernay, 2023). These benefits are particularly advantageous for complex structures and the development of novel engineering solutions.

In most cases, PBD involves using advanced analytical methods, experimental testing, or a combination of both. For advanced methods, the structural behaviour at elevated temperatures is typically predicted through nonlinear finite element analysis (NLFEA). Applying these methods to concrete structures requires comprehensive numerical models

that integrate multiple complex phenomena, such as cracking, reinforcement yielding, and material degradation due to thermal expansion. Examples of such models used to simulate RC tunnels can be found in Nieman (2008); Burggraaf et al. (2007); Noordijk et al. (2010); Van Aken (2012); Brongers (2020); Bernardi et al. (2020); Hua et al. (2022). In general, these studies demonstrate the potential of NLFEA in estimating the fire resistance of concrete structures. However, further efforts are needed to develop a consistent assessment and design verification approach in engineering practice. Particularly, specific considerations regarding the structural model and the selection of input parameters require a closer examination.

Accordingly, this study presents a systematic procedure for verifying the structural performance of RC structures exposed to fire, focusing on fire resistance duration and residual capacity. The method is exemplified using a case study which is inspired by typical rectangular cross-sections widely used in the Netherlands for immersed tunnels. Details of the approach and key outcomes are discussed in the following sections.

2 Fire design principles

Two critical considerations must be addressed when designing for fire loads: (i) ensuring sufficient time for safe evacuation before potential tunnel collapse, and (ii) protecting the asset to maintain structural repairability after the fire event. In the Netherlands, the fire design of tunnels must comply with the regulations established in the Building Decree (Bouwbesluit 2012). In addition, when designing tunnels for RWS, the following mandatory guidelines apply: National Tunnel Standard, Landelijke Tunnelstandaard (LTS) and Guidelines for special structures, Richtlijn Ontwerp Kunstwerken (ROK). The Building Decree requires sufficient time for emergency services and user evacuation before the tunnel collapses. A distinction is made between existing and new tunnels, as well as tunnels located under open water. In the case of a new immersed tunnel, the Building Decree states a fire resistance of 120 minutes.

The Building Decree refers to the Eurocodes and the respective Dutch National Annex for the structural safety of new structures. In NEN-EN 1992-1-2:2005 (2005), fire design is considered as an accidental case requiring verifications against the ultimate limit state (ULS). In a semi-probabilistic approach, the design verification adopts the following inequality:

$$R_{fi,d}(t) \geq E_{fi,d}(t) \quad \text{for} \quad t \leq t_{fi,req} \tag{1}$$

where $R_{fi,d}(t)$ is the design value of the fire resistance as a function of time; $E_{fi,d}(t)$ is the design value of an action effect in the fire situation; and $t_{fi,req}$ is the required fire resistance time. According to NEN-EN 1992-1-2:2005 (2005), Equation 1 can be verified using different methods, such as the tabulated and the isotherm 500 °C methods or advanced calculation methods, such as the finite element method.

The load combination for accidental design has the following form (load factors, γ, are set equal to 1.0):

$$\sum_{j \geq 1} G_{k,j} + P + A_d + (\psi_{1,1} \text{ or } \psi_{2,1})\, Q_{k,j} + \sum_{i>1} \psi_{2,1}\, Q_{k,i} \tag{2}$$

in which G_k, Q_k are the characteristic values of the permanent and variable actions, respectively; P refers to prestressing; A_d is the design value of the accidental action; and $\psi_{1,1}$, $\psi_{2,1}$ are the coefficients for the frequent and quasi-permanent value of variable actions, respectively, associated with the National Annex. It should be noted that, in the case of fire, the fire action cannot be represented as a static load that could be added to the other action effects. The fire action consists of indirect effects of actions in the structure by differential or restrained thermal expansion. However, evaluating these indirect effects in practice is complex and often neglected. The design values of mechanical material properties are defined as:

$$X_{d,fi} = \frac{X_k(\theta)}{\gamma_{M,fi}} = \frac{k_\theta X_k}{\gamma_{M,fi}} \tag{3}$$

where X_k and $X_k(\theta)$ are the characteristic values of the mechanical properties at normal temperature and for a temperature θ; k_θ is the reduction factor due to thermal degradation and $\gamma_{M,fi}$ the partial safety factor, which is considered equal to 1.0. As stated by Taerwe (2008), using a partial safety factor equal to 1.0 is related to the fact that there is a low probability of a fire during the structure service life. Assuming that the structure at ambient conditions meets a certain probability of failure p_f, the following inequalities can be established (*fib* Model Code 2020, 2024):

$$\begin{aligned} &P(\text{failure at ambient conditions}) \leq p_f \\ &\quad P(\text{failure in fire conditions}) \leq P(\text{there is a fire}) \cdot P(\text{failure caused by this fire}) \end{aligned} \tag{4}$$

The coupled probability of having a fire and having a failure under that fire should be the same as the probability of having a failure at ambient temperature, thus:

$$\begin{aligned} P(\text{failure at ambient conditions}) &\leq p_f \\ P(\text{failure in fire conditions}) &\leq p_f \,/\, P(\text{there is a fire}) \end{aligned} \tag{5}$$

The ROK includes additional fire resistance requirements in the design of new tunnels. In response to the problems identified regarding concrete spalling in recently built tunnels (Van der Waart van Gulik et al., 2015), RWS issued the guideline for fire-resistant structures, Richtlijn brandwerende constructies (RTD 1030, 2020). This document introduces two methods to avoid spalling in concrete linings. The so-called "simple method" requires that the temperature at the concrete surface must be limited to 100 °C through the application of a robust fire protection system. On the other hand, the "extensive method" establishes less strict temperatures, as shown in Figure 1, but requires additional guidelines and experimental verifications for the concrete mix design and the fire protection systems to ensure that spalling does not occur. It should be noted that the requirements introduced in RTD 1030 (2020) are mainly focused on guaranteeing the repairability of the tunnel after the occurrence of a major fire.

3 Case study

3.1 Overview

This section presents the fire design verification of an immersed tunnel using nonlinear analysis. The reference tunnel consists of two tubes and a central mid-gallery for maintenance and evacuation, as shown in Figure 2. The adopted geometry is inspired by typical rectangular cross-sections widely used in the Netherlands for immersed tunnels. For the analysis, concrete with a compressive strength of C40/50 and B500 reinforcing steel were adopted. The rebar layout is shown in the Annex (refer to Figure 24).

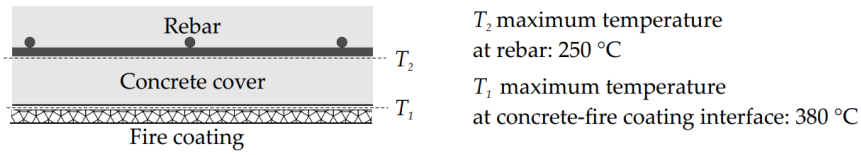

Figure 1: Temperature requirements for a tunnel under open water according to the extensive method proposed in RTD 1030 (2020)

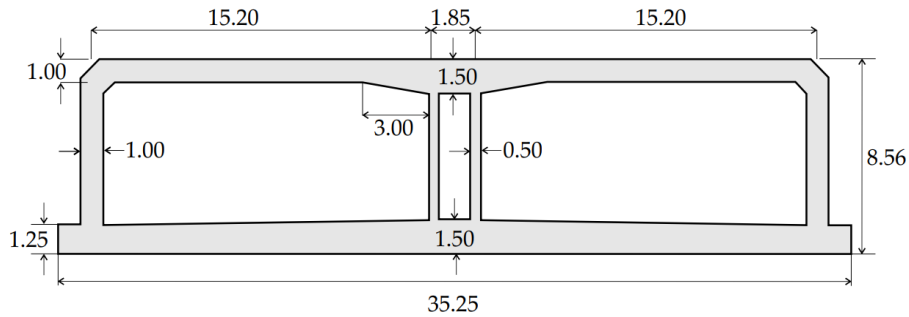

Figure 2: Cross-section geometry for reference tunnel. Dimensions in [m]

3.2 *Permanents and variables loads*

The reference tunnel is designed for the loading scenario illustrated in Figure 3. The dead weight, ballast, water pressure and ground pressure are defined as permanent loads. An additional water variation level is considered as variable load.

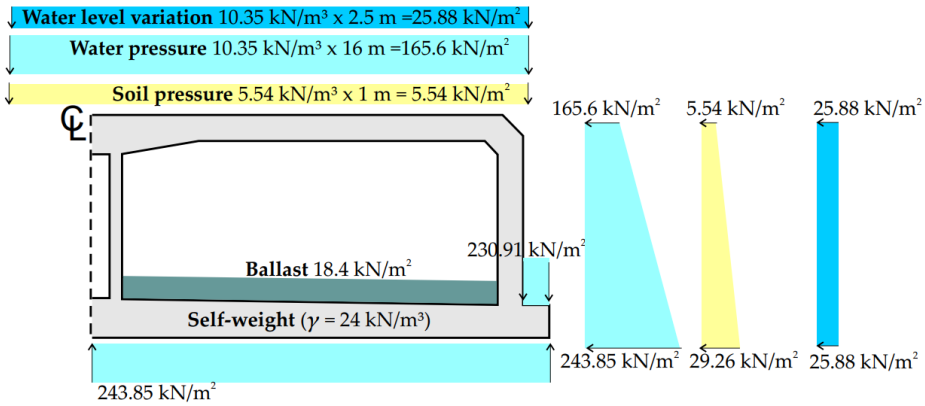

Figure 3: Permanent and variable loads considered on the reference tunnel

3.3 *Fire scenarios and analyses performed*

Due to the symmetry of the structure and the loading conditions, only one fire scenario is considered, in which the right tube in the tunnel is exposed to the RWS fire curve for 2 hours. It is noteworthy that the RWS fire curve represents a worst-case scenario, and more realistic fire scenarios can be adopted by means of computational fluid dynamics (see, for example, Bernardi et al. (2020)).

Before executing the nonlinear analyses, a linear analysis was performed to calculate the required amount of reinforcement in the tunnel cross-section according to the loads described in Section 3.2. Then, the response of the tunnel to the defined fire scenario was obtained using a performance based approach. This analysis can be interpreted as a verification of Equation 1 using NLFEA. Since this verification was originally proposed for sectional analysis and local approach methods (such as the tabulated method or the 500 °C isotherm method), modifications are proposed in this study to adapt it to a global approach using NLFEA. These modifications aim to quantify not only the fire resistance of the structure but also the residual structural capacity tunnel after a fire.

The proposed step-by-step approach is performed as follows:

1. The tunnel is simulated at ambient temperature and permanent and variable loads are applied according to the accidental combination (Equation 2) without including fire effects.
2. A thermo-mechanical analysis is executed in which the external load in step 1 is kept constant (see Figure 4a) and the thermal load is applied. If there is no full collapse at the end of the required fire scenario, the performance objectives are assumed to be met. Otherwise, alternative measures can be considered, such as increasing the fire protection layer thickness.
3. The remaining tunnel capacity is computed. For this purpose, an additional analysis is conducted by increasing the external mechanical load on the thermally damaged structure until failure. In this study, the remaining structural capacity is expressed as the additional load resisted by the thermally damaged structure in the numerical simulation. Additional analyses can be executed at specific times (t_0 ,t_1 ,..., t_n) to quantify the evolution of the structural residual capacity, as illustrated in Figure 4b. In the referred figure, two possible cases are presented depending on the fire resistance time resisted by the structure and the required fire resistance time.

The described procedure was applied to the fire protection configurations shown in Figure 5, referred to as Case 1 and Case 2. For both configurations, the modelling methodologies were identical, with the primary difference being the presence or absence of fire protection. In Case 1, a 30 mm heat-resistant cladding is applied on the roof and walls with a constant thermal conductivity of 0.175 W/m°C and a thermal capacity of 585 MJ/m^3 °C. The mentioned properties are based on commercially available calcium silicate-based

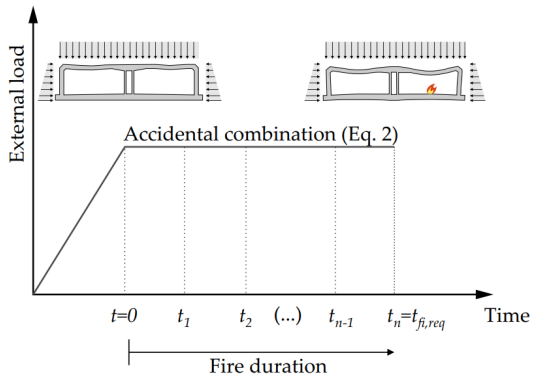

(a) Steps 1 and 2

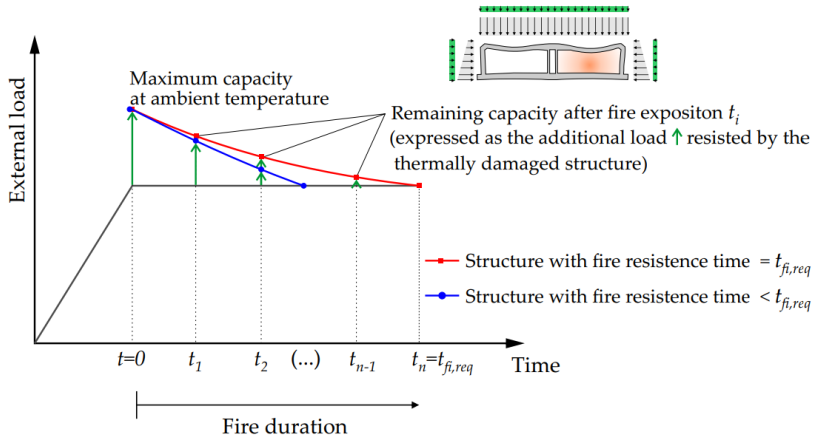

(b) Step 3

Figure 4: Procedure for verifying fire resistance using a global approach and nonlinear analysis

insulation boards (Etex NV, 2017). In the simulations, it is assumed that when fire protection is present, the concrete does not spall. Furthermore, it is assumed that the cladding remains in position during the entire fire duration. For the Case 2, the heat resistant cladding is not included. It should be noted that Case 2 does not comply with the functional requirements established in RTD 1030 (2020). This scenario was conducted only for comparison purposes and did not include an explicit simulation of concrete spalling. Figure 5c shows the RWS fire curve adopted used in the numerical models, in which the required fire resistance time is established as 120 minutes. This study only focuses on the heating phase of the fire scenario. Thus, the cooling phase and the possible residual damage during this phase are not included in the thermomechanical analysis.

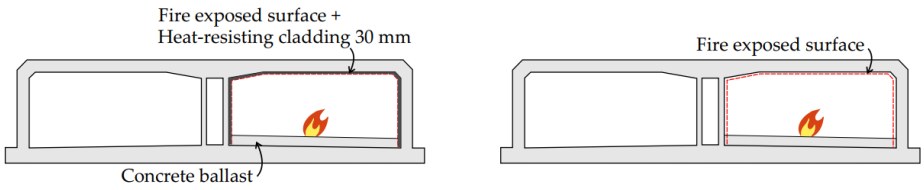

(a) Case 1 (with fire protection)

(b) Case 2 (no fire protection included)

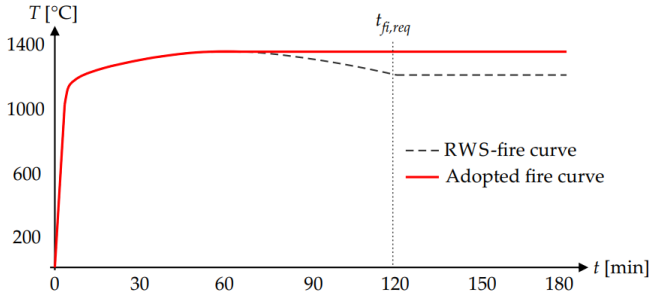

(c) RWS fire curve

Figure 5: Cases considered in the numerical analyses and fire curve adopted

Similar to traditional approaches, the application of nonlinear analyses also required the introduction of an adequate safety format to account for model, material and geometrical uncertainties. However, as mentioned in Section 2, due to the low probability of a fire during the structure service life, the use of safety factors equal to 1.0 is permitted. This study also applies this assumption to fire design verification using nonlinear analysis. In addition, the use of material properties with mean and characteristic values in the numerical simulation is compared. In both cases, the degradation of the mechanical properties as a function of the temperature is included in the numerical analysis.

4 Numerical model

4.1 Overview

The behaviour of the reference tunnel under fire is investigated using the software DIANA (version 10.8). The methodology applied for the thermo-mechanical analysis followed the recommendations developed in a previous study (Díaz et al., 2024). A staggered approach is used to perform the thermo-mechanical analysis of the tunnel cross-section. In this approach, the heat transfer is solved first, and then the temperature effects are superimposed in the mechanical analysis. The main assumption is that the temperature distribution in the structure can be decoupled from the mechanical response.

In the thermal analysis, the temperature distribution is calculated using a transient heat flow analysis. The time-dependent temperature in the fire-exposed structure can be considered as a potential convection-diffusion problem, which can be stated as:

$$\rho c_p \frac{\partial T}{\partial t} = k \nabla^2 T \tag{6}$$

where T and t denote the temperature and time, respectively; and ρ, c_p and k are the density, specific heat capacity and the conductivity of concrete, which are assumed to be temperature-dependent. The solution of Equation 6 requires the definition of initial boundary conditions, which can be prescribed to account for heat flux due to convection and radiation:

$$k \frac{\partial T}{\partial n} = -\alpha_c (T_E - T) - \varepsilon_m \, \varepsilon_f \, \sigma (T_E^4 - T^4) \tag{7}$$

in which n denotes the outward normal direction to the surface; α_c is the concrete heat transfer coefficient of the convective heat flux; T_E is the imposed time-dependent temperature on the structure; ε_m is the surface emissivity coefficient, which determines the amount of thermal radiation emitted; ε_f is the view factor between the surfaces, assumed as 1.0; and σ is the Stefan-Boltzmann constant 5.67×10^{-8} W/m^2 K^4 .

In the mechanical analysis, the temperature distribution is considered by reducing the temperature dependent material properties and by decomposing the total strain vector as follows:

$$\varepsilon_{tot} = \varepsilon_\sigma + \varepsilon_\theta \tag{8}$$

where ε_σ and ε_θ are the mechanical and thermal-induced strains, respectively; ε_θ can be decomposed again into several contributions, such as free thermal strain ε_{th} , thermal shrinkage strain ε_{sh} , and transient creep ε_{cr} :

$$\varepsilon_\theta = \varepsilon_{th} + \varepsilon_{sh} + \varepsilon_{cr} \tag{9}$$

The decomposition established in Equation 8 permits the superposition of the thermal effects with other nonlinear phenomena in concrete structures (i.e., cracking and crushing of concrete and yielding). In addition, a classical displacement-based formulation within the framework of the finite element method can be used to find the structural response, with the thermal effects superposed.

4.2 *Mesh discretisation and boundary conditions*

Continuum 2D elements are employed to discretise the immersed tunnel. A plane-strain state is considered to represent the tunnel cross-section. Therefore, the displacements in the out-of-plane direction are considered zero. Figure 6 shows the mesh and boundary conditions adopted in the simulations. Since the fire was only applied on the right tube, a more refined mesh was used in that location (average mesh size 30 mm). The mesh size was set to obtain a nonlinear temperature distribution at the concrete cover. Preliminary analyses also highlighted the importance of using a structured mesh to avoid any influence on the obtained temperature distribution in the thermal analysis. An average mesh size of 150 mm was used on the left tube.

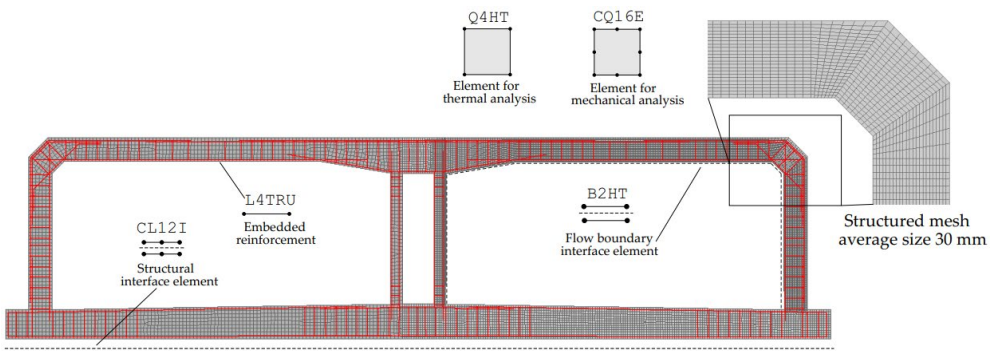

Figure 6: Typical mesh and boundary conditions used in the numerical simulations

For the staggered analysis, first-order isoparametric elements (denoted in DIANA as Q4HT) are employed for the thermal calculations. In the subsequent mechanical analysis, these elements are automatically upgraded to second-order isoparametric elements denoted as CQ16E. The use of different element types is justified by the type of interpolation required in each analysis. For the heat transfer problem, the temperature varies linearly inside the element. For the mechanical analysis, it is assumed that the strain varies linearly inside the element.

Figure 6 shows the reinforcement considered in the cross-section, derived from the loading scenario described in Section 3.2 and the corresponding internal forces diagrams (refer to Figure 25 in the Annex section). The reinforcement is represented by individual bars modelled by truss elements embedded in concrete. The embedded approach implies that the reinforcement nodes are made kinematically dependent on the concrete nodes. The

rebar geometry is assigned using an equivalent thickness based on the number of bars and spacing in the out-plane direction. The bar elements are not explicitly considered in the thermal analysis. Instead, the temperature at the reinforcement is assumed to be the same as the surrounding concrete.

In the numerical simulations, the soil is not explicitly modelled but accounted for by an elastic foundation at the bottom slab of the tunnel and loads exerted on the lateral walls and ceiling. The foundation is represented by interface elements (CL12I) with no support in tension and a high compression stiffness a high stiffness (0.05 N/mm^3). The shear stiffness was estimated at 0.02 N/mm^3 using the recommendations found in Burggraaf et al. (2007).

Heat transfer was considered through convection and radiation mechanisms using boundary interface elements (B2HT). The temperatures from the RWS fire curve were used as an input for the thermal analysis. The convection coefficient at the exposed sides was 50 W/m^2 °C. For radiation thermal transfer, an emissivity coefficient of 0.7 was used. For case 1, the fire protection was simulated with four-noded flow elements (Q4HT) with constant thermal conductivity (0.175 W/m°C) and thermal capacity (585 MJ/m^3 °C). The stiffness of the protective layer was neglected in the mechanical analysis.

*4.3 **Material constitutive model***

The constitutive model adopted for representing the reinforced concrete nonlinear behaviour at ambient temperature is summarised in Table 1.

Table 1: Concrete constitutive model at ambient temperature used in the numerical simulations

Parameter	Description
Crack model	Total Strain Fixed Crack
Tension softening	Hordijk (1991)
Compression softening	Parabolic curve, Feenstra (1993)
Compressive behaviour with lateral confinement	Hsieh et al. (1982) (four-parameter failure surface)
Compressive reduction due to lateral cracking	Vecchio and Collins (1993)
Shear modulus in cracked state	DeJong et al. (2008)

The adopted constitute model was extended for thermo-mechanical analysis by including temperature dependent evolution laws for the mechanical properties and the thermal expansion coefficients for concrete and reinforcing steel. A siliceous aggregate type was assumed to define the concrete properties according to NEN-EN 1992-1-2:2005 (2005). The relation of concrete fracture energy follows the recommendations found in Cervenka et al. (2006). A representation of the adopted laws is shown in Figure 7. The transient creep strain (also known as load-induced thermal strain, LITS) is modelled by shifting the strain at the maximum compressive stress. For the reinforcing steel, the modulus of elasticity and the yield stress are also assumed to be temperature dependent according to NEN-EN 1992-1-2:2005 (2005).

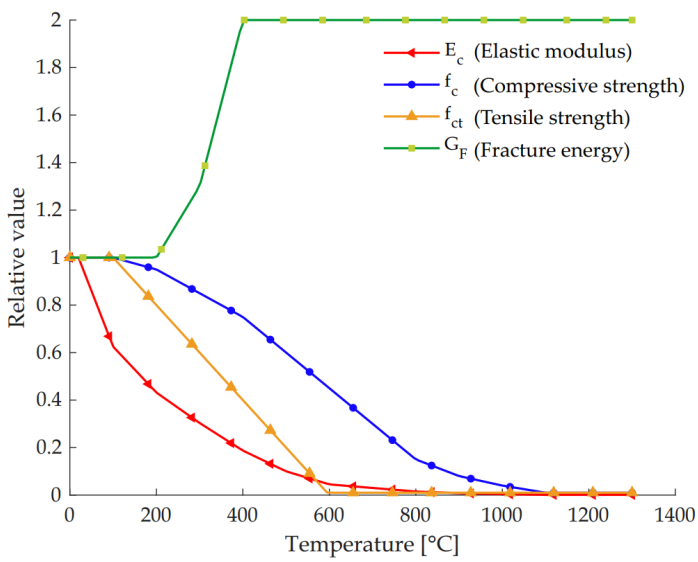

Figure 7: Temperature dependence of concrete properties

For the heat transfer analysis, concrete thermal conductivity and volumetric specific heat were defined, assuming a moisture content of 3%. These properties are also considered temperature-dependent using the relations in NEN-EN 1992-1-2:2005 (2005). An average value between the lower and upper bound limits prescribed by NEN-EN 1992-1-2:2005 (2005) is used for the thermal conductivity. As mentioned in Section 3.3, the influence of the mean and characteristic values on the numerical response is investigated in this study. The adopted input parameters for concrete and reinforcing steel are summarised in Table 2.

Table 2: Mean and characteristic values of mechanical properties in the simulations of Case 1 and 2

Parameter	Mean value	Characteristic value
Compressive strength [MPa]	48	40
Tensile strength [MPa]	3.51	2.41
Fracture energy [N/mm]	105	100
Steel yield strength [MPa]	543	500

4.4 Iterative procedure and loading sequence

The convergence parameters used for the thermal and the subsequent mechanical analysis are summarised in Table 3. The introduction of thermal and mechanical follows the step-by-step procedure described in Section 3.3. First, the permanent and variable loads were applied to the structure during the first 100 steps, and then the thermal effects were superimposed. For the computation of the structural residual capacity, a new analysis was executed on the thermally damaged structure in which the variable load was increased until failure.

5 Results

5.1 Mechanical response at ambient temperature

Figure 8 shows the crack pattern and the deformed shape of the tunnel obtained after applying the accidental load combination (before introducing thermal effects) and using the mean values presented in Table 2 as input. The crack pattern obtained in the

Table 3: Convergence parameters used in the numerical analyses

Thermal (transient heat transfer) analysis	Method	Regular Newton-Raphson
	Step size	60 seconds
	Maximum number of iterations	25
	Convergence tolerance	10^{-6}
Mechanical (structural nonlinear) analysis	Method	Regular Newton-Raphson
	Step size	30 seconds *
	Maximum number of iterations	500
	Convergence tolerance Energy	Energy 10^{-4}
		Force 10^{-2}
		Displacement 10^{-2}

* For Case 2, a step size of 15 seconds was used during the first 30 minutes of the RWS curve.

simulations is derived from the principal tensile strains at each integration point. The analysis highlights the formation of bending cracks in different regions on each tube, including the inner side of the ceiling and foundation slabs (due to sagging moments) and also on the outer side of the external walls and above the mid-gallery (due to hogging moments). In addition, early inclined cracks towards the internal wall supports are observed. The different mesh sizes adopted on each tube influenced the estimation of the crack widths, leading to a non-symmetrical pattern. In the case of the most refined mesh (30 mm), most cracks were in the range of 0 - 0.33 mm. As further discussed in Section 5.5, in general, similar numerical results were obtained using mean and characteristic values as input for Case 1.

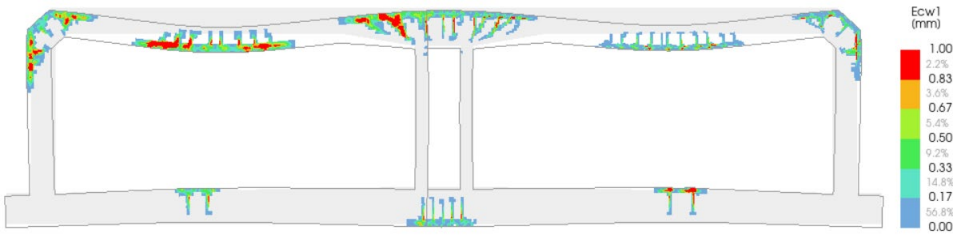

Figure 8: Crack pattern after applying accidental combination; mean values used as input (according to Table 2) (deformed shape is magnified by a factor of 20)

*5.2 **Thermo-mechanical response for Case 1 (with fire protection)***

The cracking evolution due to the thermal gradient for Case 1 (with fire protection) is shown in Figure 9. The results show that some thermal damage occurs in the tunnel even with the simulation of the fire protection and the assumption that it remains attached to the concrete for the entire duration of the fire scenario. The thermal damage is more noticeable after 120 minutes of fire exposition (Figure 9c), in which extensive cracks develop at the bottom side of the ceiling, and pre-existing cracks grow above the mid-gallery and at the corner of the external wall. This response is explained by the thermal gradient over the concrete thickness. The gradient induces additional curvatures and stresses on the heated side and, as a result, increases the hogging moments in the tunnel cross-section.

Despite the damage caused by the fire, the tunnel section maintained its stability during the required time (120 minutes), as shown in Figure 9c. For this reason, the thermo-mechanical analysis was extended for an additional hour, leading to the crack pattern

observed in Figure 9d. Once more, the cracks grow and widen with increasing fire duration, but a full collapse is discarded according to the simulation results. Figure 9d indicates extensive cracking on both middle and external walls and the formation of additional inclined cracks between the middle wall and the sagging moment region.

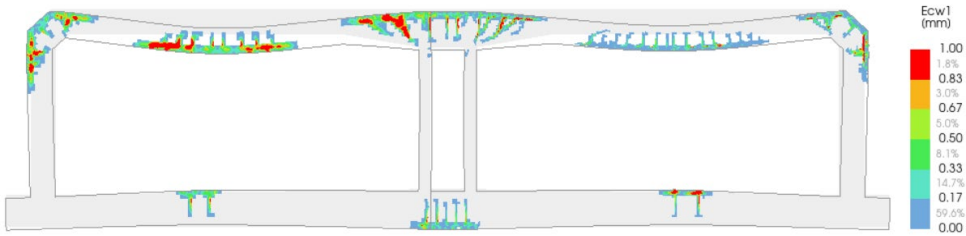

(a) crack pattern, t = 30 minutes

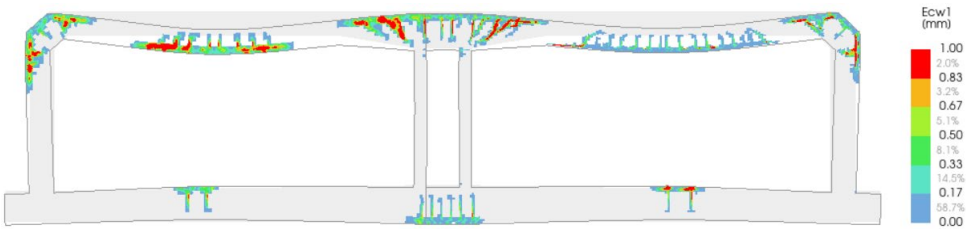

(b) crack pattern, t = 60 minutes

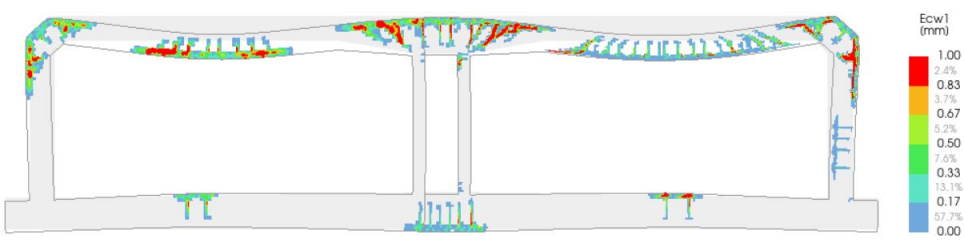

(c) crack pattern, t = 120 minutes

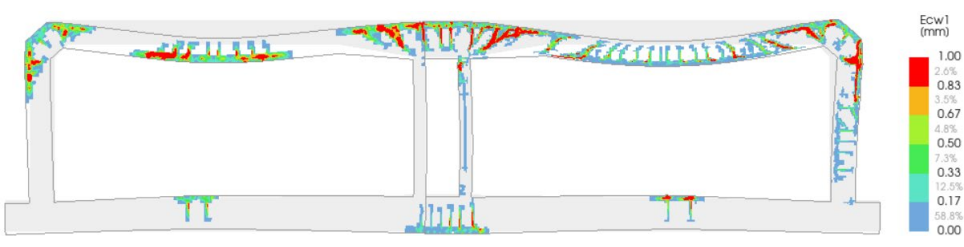

(d) crack pattern, t = 180 minutes

Figure 9: Evolution of crack pattern due to thermal loads for Case 1, with fire protection and mean values used as input (deformed shape is magnified by a factor of 20)

Figure 10 shows the number of iterations required to obtain convergence through the mechanical analysis of Case 1. A dashed line is also included to indicate the maximum number of iterations established for the analysis, as presented in Table 3. Overall, it can be seen that convergence was reached in most of the steps. Some exceptions were observed during the first steps where the rapid temperature rise of the applied fire curve can explain this behaviour. Non-convergent steps were also observed during the analysis, corresponding with the development of critical cracks in the tunnel ceiling.

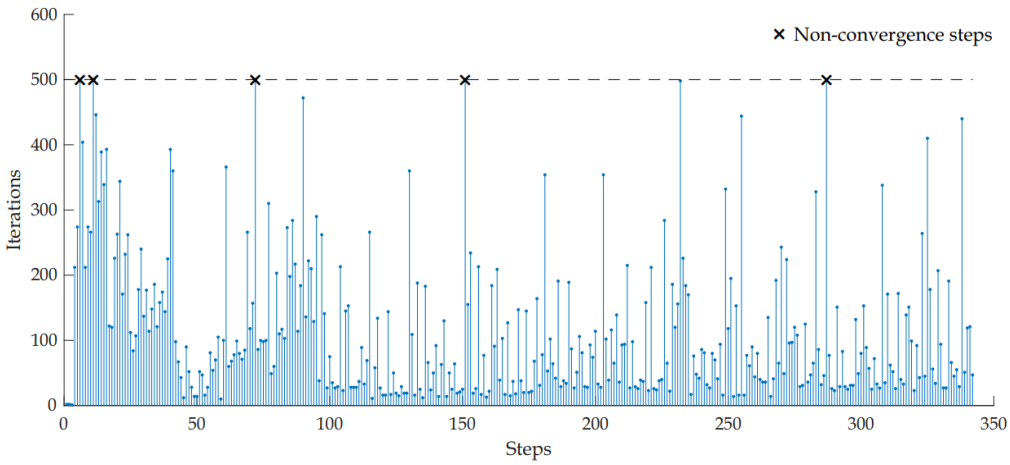

Figure 10: Convergence behaviour in the thermo-mechanical analysis of Case 1

The stresses at the reinforcement bars before and after applying the fire loads for Case 1 are presented in Figure 11. It can be seen that the application of permanent and variable loads according to Equation 2 induces stresses in the bars within the range of -200 MPa to 400 MPa. The largest values of tensile stresses are located above the middle wall and at the ceiling midspan. After 180 minutes of fire, yielding is observed at longitudinal bars located at the outer side of the hogging moment regions (external wall corner and above the middle wall). In addition, the analysis indicates the development of compressive stresses at longitudinal bars located on the exposed side of the tunnel. The stresses at the reinforcement confirmed the thermal gradient effects described in the cracking evolution. Significant yielding is also observed at the stirrups adjacent to the middle wall.

Figure 12 shows the temperature contour plots and the temperature evolution at different heights of the concrete section as a function of time. The prescribed RWS fire curve is also

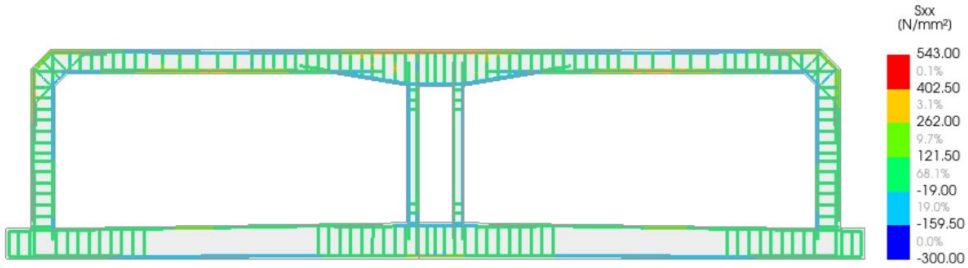

(a) Rebar stress, t = 0 minutes

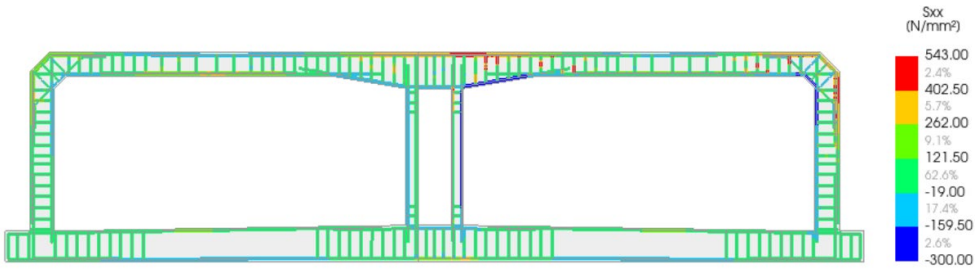

(b) Rebar stress, t = 180 minutes

Figure 11: Rebar stresses for Case 1, with fire protection and mean values used as input (according to Table)

included in the plot to highlight the performance of the fire protection in reducing the temperature at the concrete cover. The temperature distribution over the cross-section reveals a high nonlinear thermal gradient in which the maximum temperatures are localised in a 30 mm band at the concrete cover. After 120 minutes, the maximum temperature at the concrete cover is 305 °C, complying with the functional requirements of RTD 1030 (2020) (< 380 °C), illustrated in Figure 1. The maximum temperature at the rebar height was estimated at 145 °C, which also meets the temperature requirement (< 250 °C).

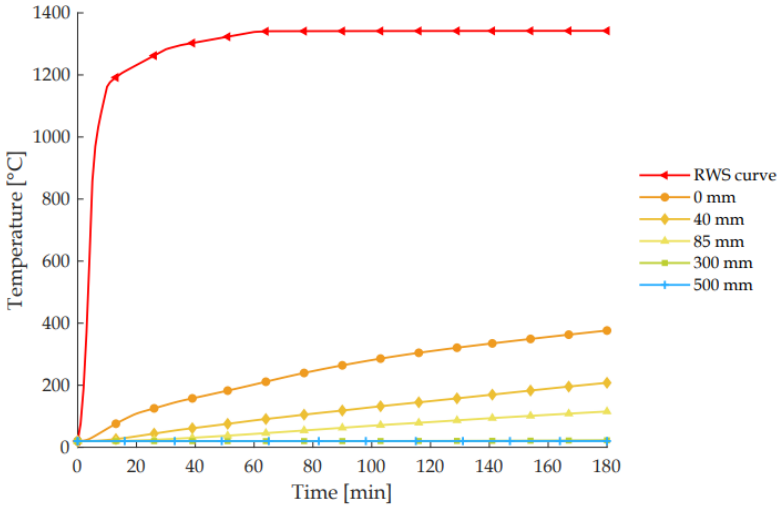

(a) Temperature evolution inside concrete located at the ceiling midspan

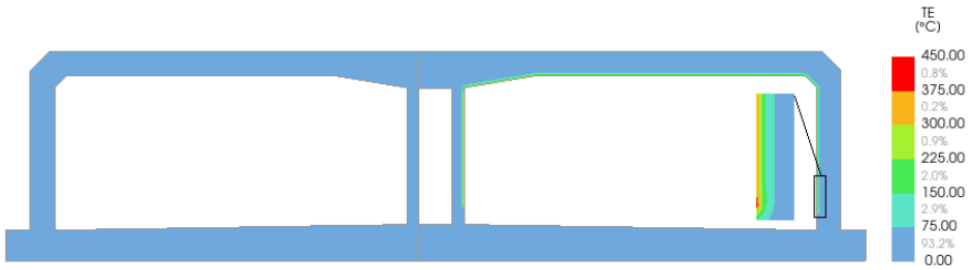

(b) Temperature contour plot, t = 180 minutes

Figure 12: Verification of functional requirements for Case 1

*5.3 **Thermo-mechanical response for Case 2 (without fire protection)***

The thermal analysis results for Case 2 are shown in Figure 13. As expected, the temperature distribution over the concrete section is significantly higher than in Case 1. The exposed concrete surface followed the RWS fire curve, and just after 5 minutes, the temperature reached 392 °C. For the reinforcement, the maximum temperature of 250 °C required by RTD 1030 (2020) was reached after 35 minutes. The contour plot presented in Figure 13b indicates that the maximum temperatures (within a range of 1125 and 1350 °C) localised to a narrow band of the concrete thickness, confirming a high thermal gradient. It is important to mention that concrete spalling was not included in the simulations.

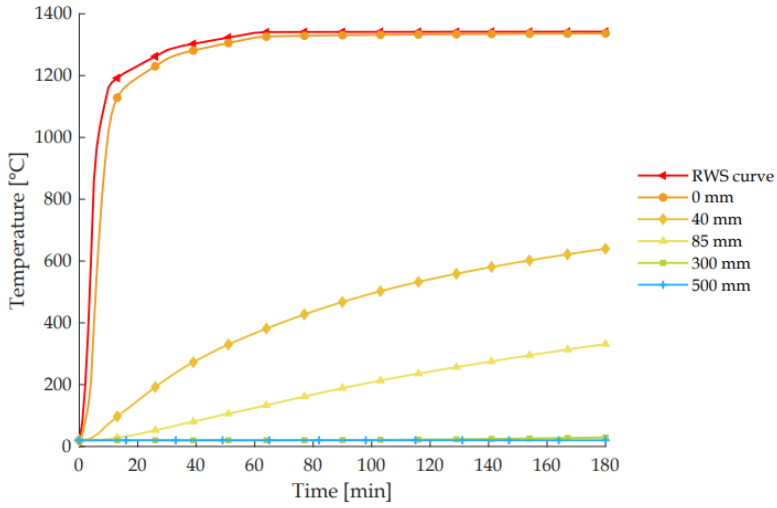

(a) Temperature t = 3h

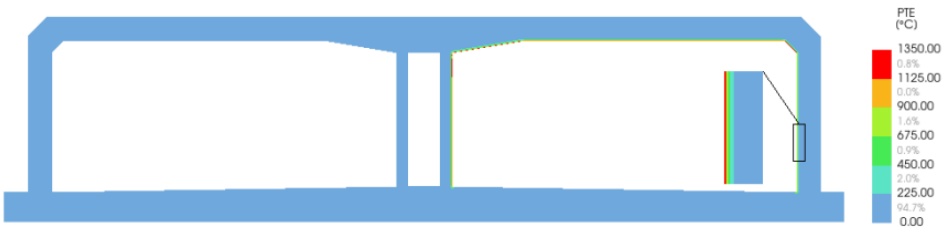

(b) Temperature at cover, t = 59 minutes.

Figure 13: Verification of functional requirements for Case 2

Numerical instabilities influenced the mechanical response and fire resistance estimation of Case 2. During the superposition of thermal effects, preliminary analyses pointed out a lack of convergence in the iterative procedure and divergence occurred after 8 minutes of fire exposure. An examination of the crack pattern and deformations obtained in the simulation show the development of unreal large localised displacements at the exposed surface, as shown in Figure 14a. This behaviour can be explained by the rapid degradation of mechanical properties at the concrete cover and the large thermal gradient previously described. Hence, the system of equations may become ill-conditioned due to multiple integration points with low stiffness. The relatively short resistance period estimated by the simulation (8 minutes), together with the lack of a clear global failure mechanism, suggests that the numerical analysis underestimates the fire resistance of the tunnel.

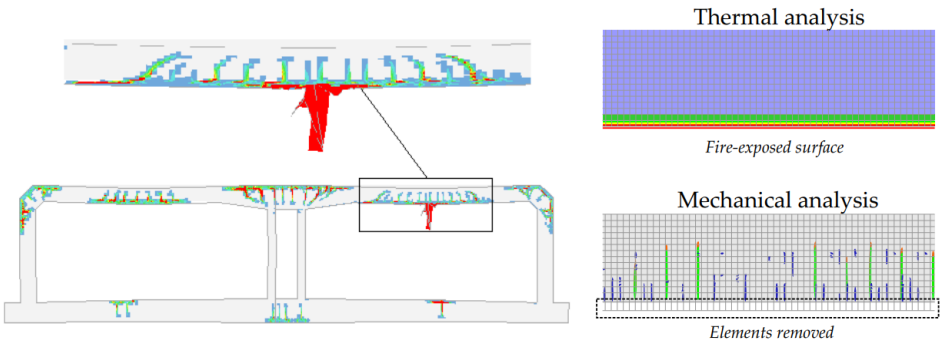

(a) Unrealistic crack pattern, t = 8 minutes (b) Proposed approach

Figure 14: Preliminaries results of Case 2 and approach to overcome numerical instabilities

The aforementioned results motivated additional modifications in the numerical model for Case 2 to reduce the numerical problems in the iterative procedure. The proposed approach neglected the mechanical stiffness of the elements located in the first row (within 30 mm) of the exposed surface, as shown in Figure 14b. Therefore, those elements were only considered as flow elements during the thermal analysis and automatically removed during the subsequent mechanical analysis. It should be mentioned that this procedure cannot be considered as explicit modelling of spalling since the contribution of the removed elements is still considered in the thermal analysis. The comparison of the mechanical response with accidental load combination (before the fire) indicated negligible differences between the original model and the one with the mentioned simplification.

The introduction of the described procedure led to a more stable convergence and an increment in the estimation of the tunnel fire resistance. Figure 15 shows the crack pattern at the last convergence step, obtained after 59 minutes of fire exposure. It is interesting to note the similarity with the crack pattern obtained for Case 1 after 180 minutes of fire (Figure 9d), with the main cracks located above the middle walls and the corner of the external wall. Similar results are also observed between the stress reached at the rebar in Figures 11b and 16.

The convergence behaviour obtained during the thermo-mechanical analysis for Case 2 is shown in Figure 17. The plot highlights the large number of iterations required to reach convergence during the first steps. After step 17, the number of iterations reduces significantly. Toward the end of the analysis, additional non-converged steps are observed,

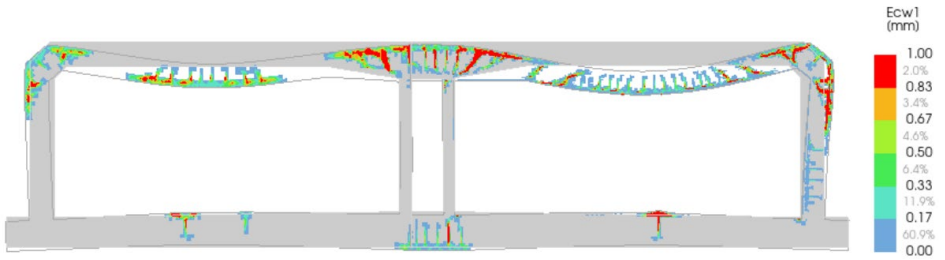

Figure 15: Crack pattern at t = 59 minutes for Case 2, mean values used as input (deformed shape is magnified by a factor of 20)

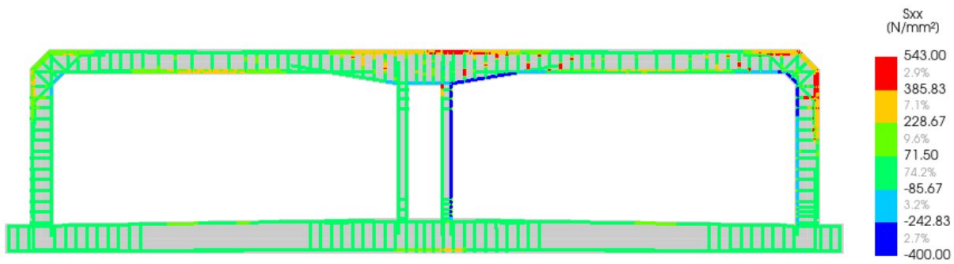

Figure 16: Stress at t = 59 minutes for Case 2, mean values used as input

and finally, divergence occurs. The extensive cracking and the considerable reduction of mechanical properties after 60 minutes of fire exposure suggest a structural failure of the tunnel cross-section. Additional results are presented in the following section to provide

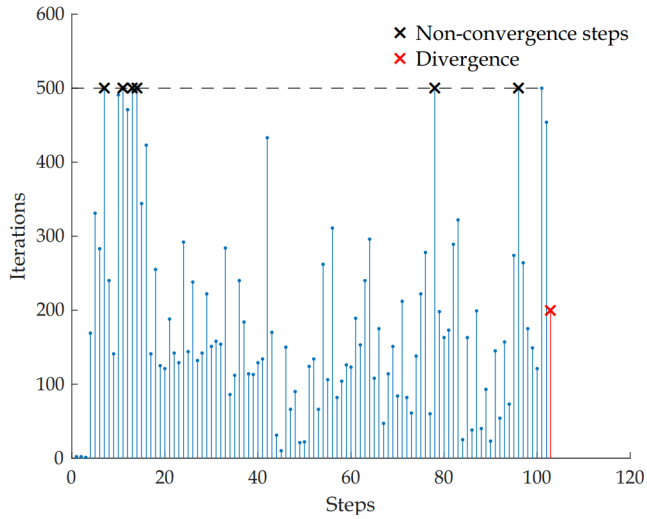

Figure 17: Convergence behaviour of thermo-mechanical analysis of Case 2

more insight into the tunnel failure behaviour. In any case, the estimated fire resistance time obtained for Case 2 should be regarded with caution, as the 2D numerical analysis neglects the possible favourable redistribution of forces in the tunnel longitudinal direction. This redistribution can increase the tunnel robustness and avoid a full structure collapse.

5.4 *Comparison of the mechanical response of Cases 1 and 2*

This section presents additional results to provide more insights into the mechanical response of Cases 1 and 2. Figures 18 and 19 show the bending moment and shear forces diagrams at the tunnel ceiling after 59 minutes of fire exposure, corresponding to the predicted fire resistance time of Case 2. The influence of fire protection is highlighted by

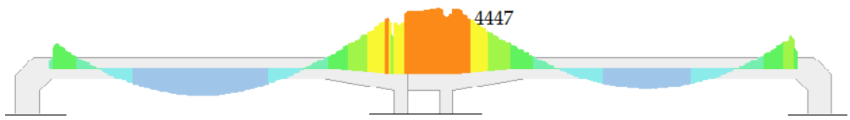

(a) Case 1, t = 59 minutes

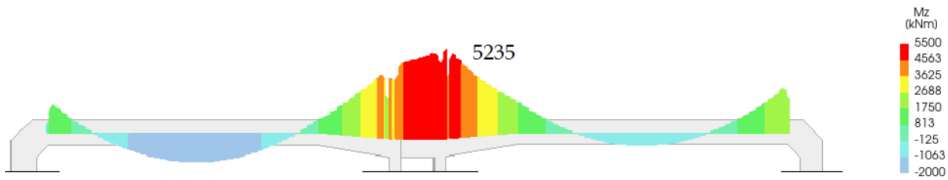

(b) Case 2, t = 59 minutes

Figure 18: Bending moment diagrams at the ceiling for Cases 1 and 2 after 59 minutes of fire exposure

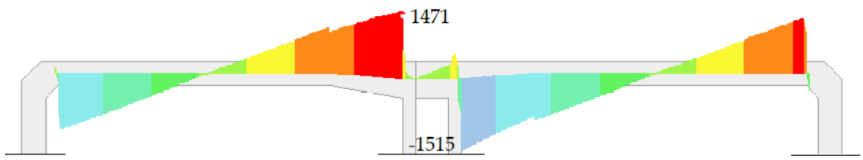

(a) Case 1, t = 59 minutes

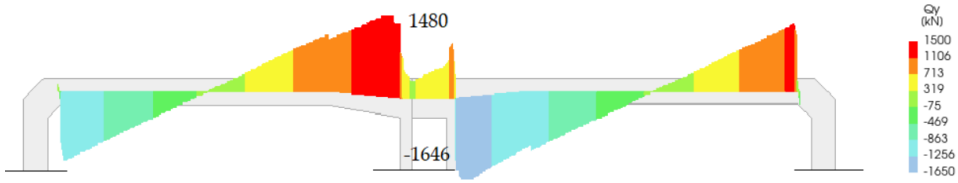

(b) Case 2, t = 59 minutes

Figure 19: Shear forces diagrams at the ceiling for Cases 1 and 2 after 59 minutes of fire exposure

the redistribution and maximum bending moment values observed in Figure 18. For Case 2, a large redistribution is noted, leading to higher bending moment values at the hogging region, above the middle walls, and a reduction of the moment at the midspan. Less redistribution is observed in the case of shear forces, where similar values for both cases can be observed in Figure 19.

Figure 20 shows the evolution of the bending moments at the hogging and sagging regions for both cases and highlights the effect of the fire protection on the mechanical response of the tunnel cross-section. Above the middle wall, the bending moment value after applying the mechanical loads is around 4200 kNm (refer to Figure 20a). The superposition with the thermal effects rapidly increases the bending moment in Case 2 until 59 minutes of fire exposure, where the last converged step was reached in the analysis. For Case 1, the fire protection leads to a smaller moment rate increase due to the presence of fire protection. Similar bending moment values are observed after one hour and three hours of fire exposure for Case 1 and Case 2 (around 5200 kNm), respectively. A similar trend is observed at the midspan, as shown in Figure 20b.

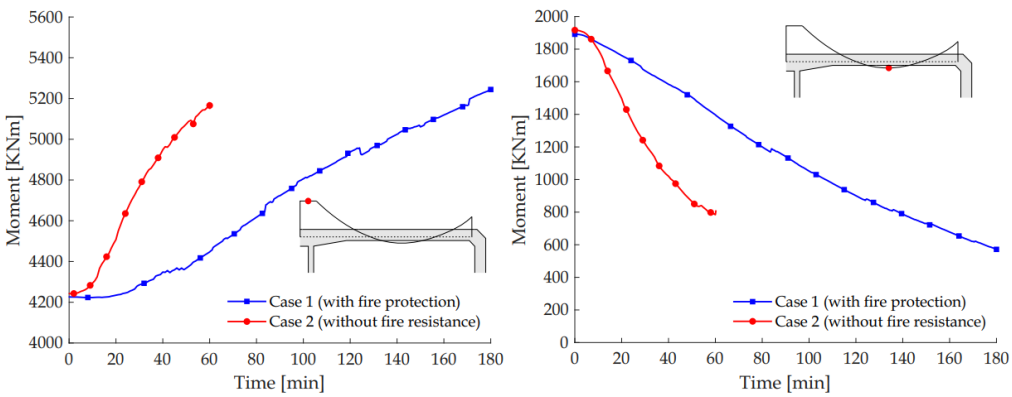

(a) Moment above middle wall *(b) Moment at midspan*

Figure 20: Evolution of bending moments at the ceiling as a function of the fire exposure time

The evolution of the rebar stresses at the longitudinal rebar, and the shear reinforcement is presented in Figure 21. The comparison is limited to the locations where the largest values were found during the analyses. Figure 21a shows a similar behaviour to the one described for Figure 20a, indicating a rapid rise for Case 2 compared to Case 1. Figure 21b indicates the activation of the shear reinforcement, which is closely related to the sudden

development of inclined cracks at the tunnel ceiling. The presence of fire protection delays this phenomenon for about one hour, as shown in the stress evolution obtained for Case 1. In addition, it can be noted that the Case 2 analysis ended shortly after the shear activation. Thus, it can be assumed that the combination of shear cracks with the reduction of the mechanical properties due to fire led to the divergence observed at the end of the iterative procedure. For case 1, the analysis maintained a stable convergence behaviour after the activation of the shear reinforcement, indicating less fire-induced damage within the concrete thickness.

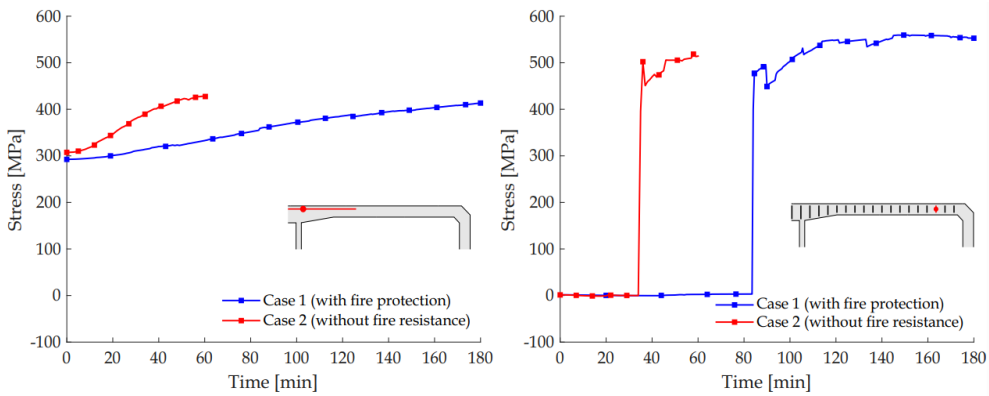

(a) Longitudinal rebar *(b) Shear reinforcement*

Figure 21: Evolution of rebar stresses as a function of the fire exposure time at indicated locations

The mechanical response of Cases 1 and 2 is also compared in terms of the maximum vertical displacements obtained in the analyses, as shown in Figure 22. This comparison confirms the favourable response obtained with the application of fire protection. In this case, the deflection ratio is reduced significantly, and almost no change in the tunnel deflection at the midspan is observed within the first hour of fire exposure. Then, the deflection rate increases at a lower rate compared to Case 2.

5.5 Assessment of remaining structural capacity

Figure 23 summarises the evolution of the tunnel structural capacities for Cases 1 and 2 as a function of the time exposure. The results for the analyses with mean and characteristic values are also compared in the referred plot. The external vertical load corresponding to the combination of permanent and variable loads (Equation 2) is included as a dashed line and is equal to 10.3 MN. Since this load was kept constant during the thermo-mechanical analysis, it is used as a reference for calculating the residual capacity.

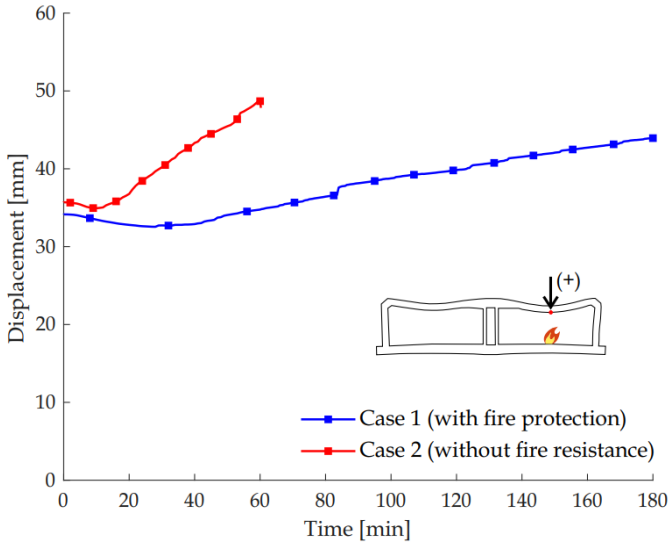

Figure 22: Evolution of displacements at the ceiling midspan

As mentioned in Section 3.3, additional analyses were executed on the thermally damaged tunnel to quantify the evolution of the structural residual capacity. The remaining capacity is expressed as the additional load resisted by the thermally damaged structure in the numerical simulation. For $t = 0$, the total external load resisted by the tunnel corresponds to the ultimate capacity at ambient temperature. According to the numerical models, the ultimate capacity of the tunnel was 14.5 MN and 13.9 MN for the input with mean and characteristic values, respectively.

For Case 1, the evolution of the residual structural capacity decreased as a function of time, with relatively stable periods between 30 and 60 minutes and after 120 minutes. As mentioned, the tunnel did not lose its structural integrity during the required time, and the calculation was extended up to 180 minutes. By the end of the analysis, the capacity of the tunnel cross-section was reduced by approximately 10% in comparison with the capacity calculated at ambient temperature, and the residual capacity of the tunnel was estimated at 13.1 MN and 12.4 MN for the input with mean and characteristic values, respectively.

For Case 2, where no fire protection was included, a more rapid degradation was obtained. Different from Case 1, the adoption of mean and characteristic led to a difference in the estimation of the fire resistance time, corresponding to 31 and 59 minutes for the input

with mean and characteristic values, respectively. Since the analyses stopped before reaching the required fire resistance time (120 minutes), no additional load could be applied in the numerical models. Thus, it is assumed that the residual capacity corresponds to the imposed load combination (10.3 MN).

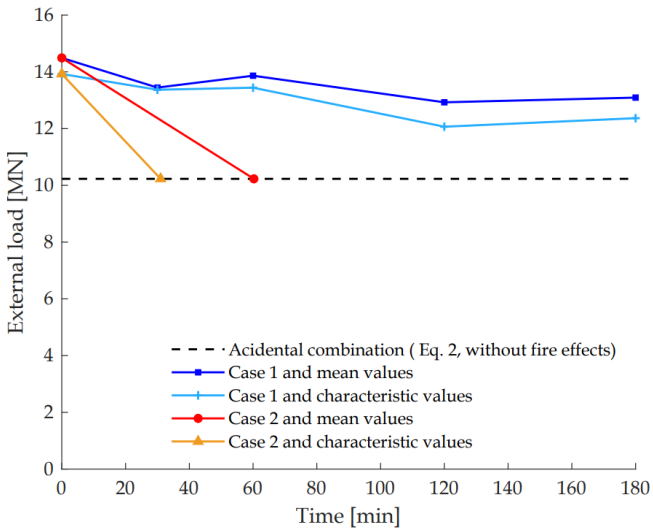

Figure 23: Assessment of remaining structural capacity for Cases 1 and 2

6 Discussion

The results show the capabilities of using NLFEA to verify the temperature requirements and trace the damage with increasing fire duration. The evolution of the crack pattern and stresses at the rebar are aligned well with the moment redistribution at the sagging and hogging moment regions. The obtained structural behaviour is in agreement with previous experimental (Duan et al., 2021; Dong et al., 2023; Lin et al., 2021) and numerical (Burggraaf et al., 2007; Nieman, 2008; Van Aken, 2012) observations of tunnels with a similar cross-section. In particular, the formation of cracks on the outer (unheated) side of the tunnels which may have important implications for the service life and repairability of immersed tunnels is pointed out.

The results obtained in Cases 1 and 2 justify using fire protection for a worst-case scenario such as the RWS fire curve. The simulations showed that the heat-resistant cladding delayed the damage induced by the thermal gradient. The approach proposed in this study

can also be used with more realistic fire loads to derive more tailored solutions. Nevertheless, additional attention has to be paid to the modelling choices adopted in this study. For example, the use of 2D continuum elements ignores the possible redistribution of internal forces in the longitudinal direction of the tunnel, which has a favourable effect on the robustness of the tunnel. The incorporation of thermal spalling and residual strains during the cooling phase should be further investigated.

7 Conclusions

This study investigates the fire performance of an immersed tunnel using nonlinear analysis. A novel approach is proposed to estimate the fire resistance time and the global structural residual capacity using NLFEA. To this end, the total strain model implemented in DIANA is extended to account for the influences of thermal effects using a staggered approach. Based on the results achieved in this study, the following conclusions can be drawn:

1. The heat transfer analysis confirms the development of significant thermal gradients over the thickness of the concrete section. Consequently, additional stresses and redistribution of internal forces occur in the structure. The incorporation of these indirect effects cannot be ignored in the fire design of tunnels, even if fire protection is used.

2. The application of fire protection and compliance with the temperature requirements significantly influence the time fire resistance and the damage evolution of reference tunnel. However, despite the use of fire protection, considerable damage may occur during the fire event. According to the results in Case 1, it is unlikely that this damage led to a full collapse, but the crack formation at the outer side can reduce the tunnel service life.

3. Convergence instabilities due to the rapid degradation of concrete properties at the cover may arise in the thermo-mechanical analysis. These instabilities can be overcome by using a refined mesh and neglecting the stiffness of elements adjacent to the exposed surface in the mechanical analysis.

4. The use of characteristic values instead of mean values influenced the estimation of the fire time resistance when no fire protection was applied. More studies are required for the definition of an adequate safety format in the context of concrete fire design using nonlinear analysis.

The fire design verification of a concrete structure involves different uncertainties that require additional examination (i.e., fire loads and spalling rates, among others). Therefore, combining the approach proposed in this study with probabilistic methods should be further explored. This combination will be helpful in the adoption of a fire performance design approach for concrete structures.

Acknowledgments

This study was supported by Rijkswaterstaat (Dutch Ministry of Infrastructure and Water Management) through the research project "Brandwerendheid Landtunnels". The authors gratefully acknowledge this support.

References

P. Bernardi, E. Michelini, A. Sirico, S. Rainieri, and C. Corradi. Simulation methodology for the assessment of the structural safety of concrete tunnel linings based on cfd fire–fe thermo-mechanical analysis: a case study. *Engineering Structures*, 225:111193, 2020.

Bouwbesluit 2012. https://rijksoverheid.bouwbesluit.com/Inhoud/docs/wet/bb2012/hfd4. Accessed: 30-09-2024.

B. Brongers. Shear behaviour of tunnels subjected to fire: A numerical analysis of the heinenoordtunnel. Master's thesis, Delft Technical University, 2020.

H. Burggraaf, A. Overbeek, and A. Vervuurt. Repareerbaarheid van tunnels analyse van de wijkertunnel met een schijfmodel in DIANA. TNO Report 2007-D-R1204/A, 2007.

J. Cervenka, J. Surovec, P. Kabele, T. Zimmerman, A. Strauss, and K. Bergmeister. Numerical simulation of fracture and damage in rc structures due to fire. *Fracture Mechanics of Concrete and Concrete Structures*, 2:727–735, 2006.

M. J. DeJong, M. A. Hendriks, and J. G. Rots. Sequentially linear analysis of fracture under non-proportional loading. *Engineering Fracture Mechanics*, 75(18):5042–5056, 2008.

R. Díaz, E. Lantsoght, and M. Hendriks. Structural behaviour of tunnels exposed to fire using numerical modelling strategies. *Fire Safety Journal*, 2024. ISSN 0379-7112. doi: https://doi.org/10.1016/ j.firesaf.2024.104335.

Y. Dong, J. Duan, D. Zhang, J. Liu, S. Zhu, and J. Qi. Experimental research on fire resistance of the reduced scale immersed tunnel with fire in both traffic tubes. *Tunnelling and Underground Space Technology*, 132:104922, 2023.

J. Duan, Y. Dong, J. Xiao, D. Zhang, W. Zheng, and S. Zhang. A large-scale fire test of an immersed tunnel under the protection of fire resistive coating. *Tunnelling and Underground Space Technology*, 111:103844, 2021.

Etex NV. PROMATECT-H, technical data sheet. https://media.promat.com/pd36273/original/-14737322/promatect-h_tds_en.pdf, 2017. Accessed: 01.09.2024.

P. H. Feenstra. *Computational aspects of biaxial stress in plain and reinforced concrete*. PhD thesis, TU Delft, Delft University of Technology, 1993.

fib Model Code for concrete structures 2020. *fib* Model Code 2020, Lausanne, Switzerland, 2024.

T. Gernay. Performance-based design for structures in fire: Advances, challenges, and perspectives. *Fire Safety Journal*, page 104036, 2023.

D. Hordijk. *Local Approach to Fracture of Concrete*. PhD thesis, Doctoral Thesis. Delft University of Technology, Delft, The Netherlands, 1991.

S. Hsieh, E. Ting, and W. Chen. A plastic-fracture model for concrete. *International Journal of Solids and Structures*, 18(3):181–197, 1982.

N. Hua, N. E. Khorasani, and A. Tessari. Numerical modeling of the fire behavior of reinforced concrete tunnel slabs during heating and cooling. *Engineering Structures*, 258:114135, 2022.

Landelijke Tunnelstandaard (LTS). Versie 1.2 inclusief SP2 B4, Januari 2023.

J. Lin, Y. Dong, J. Duan, D. Zhang, and W. Zheng. Experiment on single-tunnel fire in concrete immersed tunnels. *Tunnelling and Underground Space Technology*, 116:104059, 2021.

NEN-EN 1992-1-2:2005. Eurocode 2: Design of concrete structures Part 1-2: General rules - Structural fire. CEN, 2005.

B. Nieman. Cracking on the unheated side during a fire in an immersed tunnel. Master's thesis, Delft Technical University, 2008.

L. Noordijk, P. Scholten, A. Breunese, and C. Both. Emerging problem for immersed tunnels: fire-induced concrete cracking. In *4th International Symposium on Tunnel Safety and Security*, pages 211– 222, 2010.

Richtlijn brandwerende constructies (RTD 1030, 2020). Rijkswaterstaat technisch document, versie 3.0, 2020.

Richtlijn Ontwerp Kunstwerken (ROK). Rijkswaterstaat technisch document, RTD 1001:2021, December 2021.

L. Taerwe. Fire design of concrete structures according to the Eurocodes: a review. In *ACI spring Convention: Designing concrete structures for fire safety*, pages 75–95. ACI, 2008.

S. van Aken. Cracking at the unheated side of a tunnel during the heating and cooling phase of a fire. Master's thesis, Delft Technical University, 2012.

R. van Coile, B. Jovanović, R. K. Chaudhary, X. Deckers, and A. Lucherini. Simplified modelling of ´ the performance of concrete tunnels during fire and post-fire damage classification. *Acta Polytechnica* CTU Proceedings, 36:253–260, 2022.

T. van der Waart van Gulik, A. Breunese, R. Jansson, L. Boström, and E. Annerel. Spalling behaviour ¨ of a non-spalling qualified concrete. In *4th International Workshop on Concrete Spalling due to Fire Exposure*, October 8-9, 2015, Leipzig, Germany, 2015.

F. J. Vecchio and M. P. Collins. Compression response of cracked reinforced concrete. *Journal of Structural Engineering*, 119(12):3590–3610, 1993.

Annex

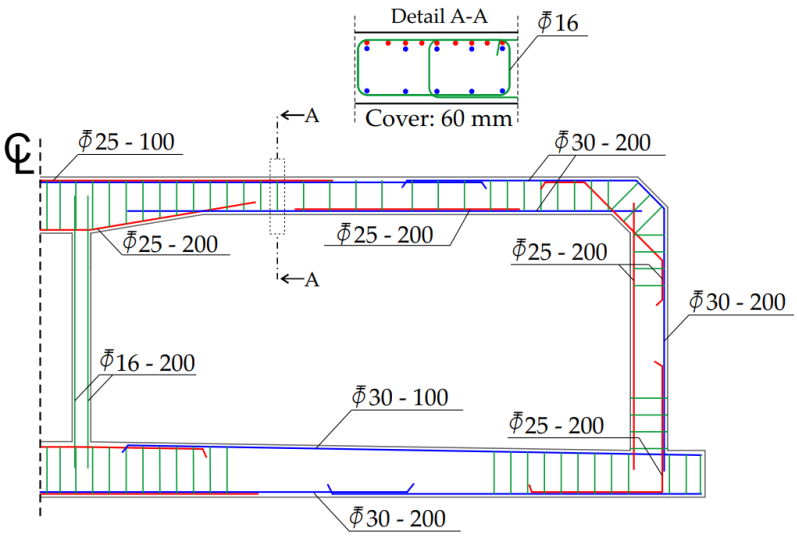

Figure 24: Rebar detailing for reference immersed tunnel analysis

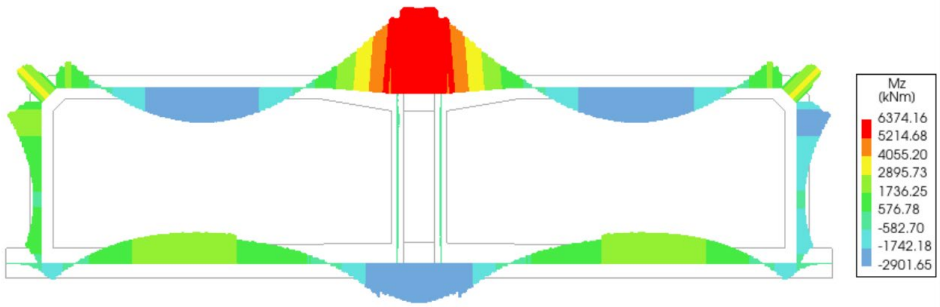

(a) Bending moment

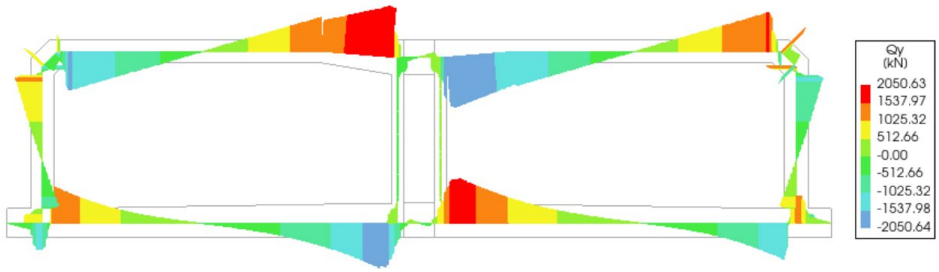

(b) Shear force

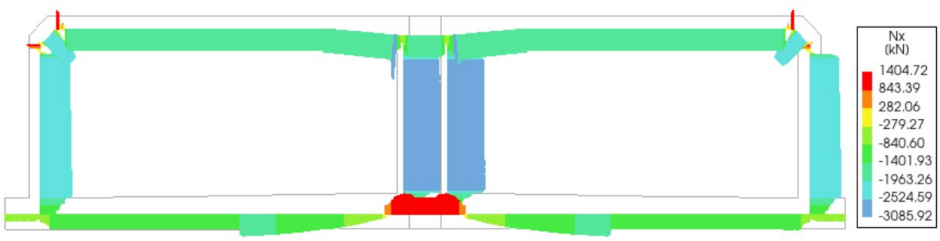

(c) Normal force

Figure 25: Internal forces for ultimate limit state verification